

# Bioinspired Smooth Neuromorphic Control for Robotic Arms

Ioannis Polykretis<sup>1,2</sup>, Lazar Supic<sup>2</sup>, and Andreea Danielescu<sup>2</sup>

**Abstract**—Replicating natural human movements is a long-standing goal of robotics control theory. Drawing inspiration from biology, where reaching control networks give rise to smooth and precise movements, can narrow the performance gap between human and robot control. Neuromorphic processors, which mimic the brain’s computational principles, are an ideal platform to approximate the accuracy and smoothness of such controllers while maximizing their energy efficiency and robustness. However, the incompatibility of conventional control methods with neuromorphic hardware limits the computational efficiency and explainability of their existing adaptations. In contrast, the neuronal connectome underlying smooth and accurate reaching movements is effective, minimal, and inherently compatible with neuromorphic processors. In this work, we emulate these networks and propose a biologically realistic spiking neural network for motor control. Our controller incorporates adaptive feedback to provide smooth and accurate motor control while inheriting the minimal complexity of its biological counterpart that controls reaching movements, allowing for direct deployment on Intel’s neuromorphic processor. Using our controller as a building block and inspired by joint coordination in human arms, we scaled up our approach to control real-world robot arms. The trajectories and smooth, minimum-jerk velocity profiles of the resulting motions resembled those of humans, verifying the biological relevance of our controller. Notably, our method achieved state-of-the-art control performance while decreasing the motion jerk by 19% to improve motion smoothness. Our work suggests that exploiting both the computational units of the brain and their connectivity may lead to the design of effective, efficient, and explainable neuromorphic controllers, paving the way for neuromorphic solutions in fully autonomous systems.

## I. INTRODUCTION

Diverse robotic applications such as prosthetics [1], assistive robotic arms [2], and industrial arms in assembly lines [3] require effective controllers that need to not only be accurate but also to provide smooth control. Beyond engineering benefits such as slowing down motor wear [4], smooth motion ensures comfort for the user and safety for the robot and the environment. Prosthetics require smooth trajectories during goal-reaching to ensure a user-friendly experience and to avoid damage to the robot or the environment [5]. Upper-limb rehabilitation robots specifically target the re-development of smooth velocity profiles for reaching movements that have been affected by diseases [6]. For industrial robotic arms, smooth control is crucial to avoid abrupt link movements that can be dangerous when interacting with the environment [7] and which could induce collisions with other agents [8]. All these applications can

significantly benefit from neuromorphic computing, which can combine smooth motion with low latency, robustness, and potentially higher accuracy [9], [10]. To leverage this emerging computing paradigm, spiking neural networks (SNNs) are used for processing on neuromorphic hardware, obeying its asynchronous and event-based computational principles [11], [12]. However, the distinctive computational principles of neuromorphic hardware are challenging for the design of diverse, low-level control behaviors. While effective SNN solutions exist for diverse, high-level tasks [13], [14], current neuromorphic controllers either disregard control smoothness [15], [16], or approximate it using large networks derived from conventional control methods [17], limiting the efficiency of neuromorphic implementations.

In contrast, the brain achieves smooth limb movements seemingly effortlessly with remarkable accuracy in the presence of limited energy and computational resources [18]–[20]. A large number of neuroscientific studies have attempted to understand the biological mechanisms behind the smooth trajectories of goal-oriented movements [21], [22]. Smooth movements of primates are driven by the regulation of the sensory feedback provided to the motor neurons through a process known as presynaptic inhibition [22]. Translating such biological principles to neuromorphic networks can give rise to robotic solutions that are not only as effective as their conventional counterparts but also efficient with respect to network size, adaptable to a wide range of stimuli, and explainable in terms of behavior and malfunction [23]–[25]. Therefore, in this work, we leverage the understanding of how the brain yields smooth movements to develop a compact SNN architecture that draws inspiration from biological findings [22] to regulate the sensory feedback provided to the motor neurons and allow for smooth and

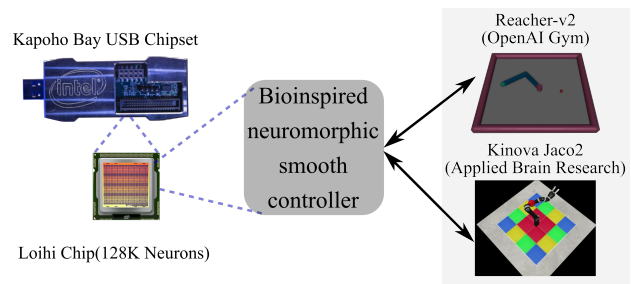


Fig. 1. Overview. An SNN-based controller inspired by the biological neuronal networks that control reaching movements provided smooth and accurate control of robot arms. The network was tested on a CPU and deployed on Intel’s Loihi neuromorphic chip to drive the end-effector of two increasingly complex simulated robot arms. The resulted control compared favorably with a state-of-the-art PID, in both smoothness and accuracy.

IP was partially funded by the Onassis Foundation Scholarship  
<sup>1</sup>Department of Computer Science, Rutgers University, New Jersey  
 ip211@rutgers.edu  
<sup>2</sup>Accenture Labs, San Francisco, California

accurate neuromorphic control.

Our SNN architecture comprises antagonistic extensor and flexor motor neurons that modify the controlled variable and sensory proprioceptor (*PPC*) neurons that ensure smoothness by regulating the sensory feedback to the motor neurons. This biologically plausible architecture allows us to directly deploy our controller on Intel’s neuromorphic research processor, the Loihi. We applied our SNN controller to two increasingly complex robotic arms (Fig. 1): i) a two-link arm (Reacher-v2), and ii) a 6-DOF real-world robotic arm (Jaco) and evaluated its effectiveness in applications that require smooth control. We show that our controller matches the performance of a conventional PID controller when evaluated on standard controller metrics (rise time, settling time, and overshoot) while also improving control smoothness. The combination of smooth control for each joint with a biologically inspired coupling of the joints gives rise to end-effector trajectories that resemble those of human arms. Therefore, our work demonstrates that biological principles can be exploited to reduce the complexity of neuromorphic solutions and achieve diverse behaviors.

## II. RELATED WORKS

Conventional control methods have matured over several decades and are now very effective for controlling joints of multi-link robotic arms. The theoretical underpinnings of these methods rely on systems of nonlinear differential equations or dynamical systems [26], [27]. The continuous, high-precision and synchronized computations that these methods rely on hinder their compatibility with modern neuromorphic processors. This incompatibility prevents them from exploiting the energy efficiency, low latency, and robustness provided by neuromorphic computing.

In an effort to combine the performance of conventional methods with the benefits of neuromorphic computing, recent solutions have attempted to translate PID controllers on both analog [28] and digital [29], [30] neuromorphic processors. Although these approaches achieve competitive control performance, they suffer in terms of computational efficiency and interpretability. These come as a necessary sacrifice when the precise, continuous values of conventional control methods need to be represented and used in the low-precision, discrete and asynchronous computations performed on neuromorphic hardware. Specifically, these approaches represent continuous values utilizing large neuronal populations, whose size scales as a function of the required control precision to allow for distinct value representation [17], [29], [30]. After encoding the continuous quantities, these methods perform the necessary computations by exploiting large neuronal arrays, further increasing the computational burden [16], [29], [31]. The large number of required components introduces significant parameter tuning, which is inefficient or even infeasible in hardware such as mixed signal neuromorphic processors with inherent inaccuracies [31]. Lastly, the resulting architectures are platform-specific [28], requiring a complete rethinking of their design to translate to different processors.

This work addresses some of these drawbacks by proposing a biologically inspired SNN for the smooth control of robotic joints. Our architecture draws inspiration from the experimentally identified neuronal connectivity that gives smooth reaching movements in rodents [22] and primates [21]. Mimicking the connectivity of its biological counterpart, our controller architecture is not only minimal in terms of computational resources but is also interpretable. Moreover, our controller is directly deployable on neuromorphic hardware.

## III. METHODS

The objective of the SNN controller is two-fold: i) to ensure control accuracy by decreasing the control error, i.e. the difference between the current control variable value  $\theta$  and the desired control variable value,  $\theta^d$ , and ii) to ensure smooth control through a gradual initial increase of the control variable and a timely steady decline to avoid overshooting the target. The architecture of the controller is shown in Fig. 3. In the following sections, we first provide a detailed description of the components of the single-joint controller and then, we describe the neuromorphic deployment of our network. Finally, we explain the addition of joint coordination to support multi-DOF arms.

### A. Architecture of the 1-DOF SNN controller

1) *Input and Feedback Encoding*: Our SNN controls a single variable by comparing its actual value  $\theta$ , which is internally fed back, with the desired value  $\theta^d$ , which is the only external input provided to the controller. The values of these two quantities are encoded into currents by the current converter modules (CCMs) and then stimulate the neurons of the network, driving their spiking activity. A pair of CCMs with opposite-signed inputs is employed for each quantity to allow for the encoding of both positive and negative magnitudes. We chose a Rectified Linear Unit (ReLU) transfer function for the CCMs to generate a positive current value when their input is positive while providing no output otherwise. In that way, the activity of the two CCM pairs is mutually exclusive since each quantity could be either positive or negative. The output currents of the CCMs were then passed to the sensory part of the network consisting of *PPC* neurons. The *PPC* neurons of our network responsible for sensing the control error and the rate of change in the control variable were then connected to the actuation component of the network, which updated the control variable to decrease the error.

2) *Sensing and Computing*: All neurons in our SNN were simulated using the leaky-integrate-and-fire (LIF) model, governed by the following dynamics:

$$u_i^{(t)} = u_i^{(t-1)} \cdot d_u + \sum_j w_{ij} \cdot s_j^{(t-1)} \quad (1)$$

$$v_i^{(t)} = v_i^{(t-1)} \cdot d_v + u_i^{(t)} \quad (2)$$

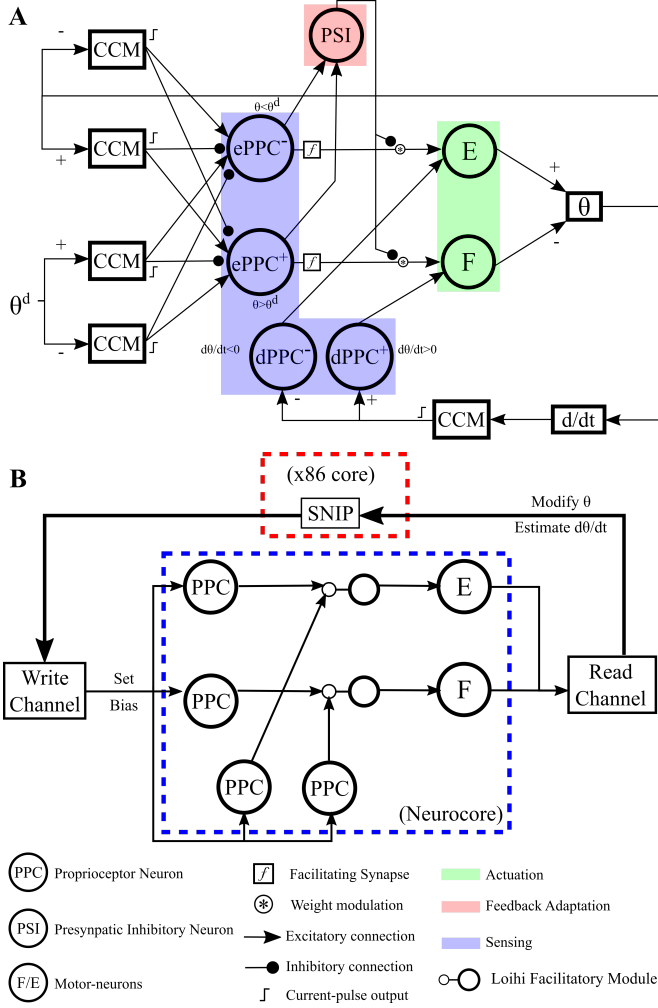


Fig. 2. SNN controller Architecture. A. CPU-based implementation. B. Implementation on neuromorphic hardware (Intel’s Loihi).

where  $t$  is the time step,  $u_i$  is the neuron’s input current,  $v_i$  is the neuron’s voltage,  $d_u$  and  $d_v$  are current and voltage decay factors,  $w_{ij}$  are the connection weights between the presynaptic neuron  $j$  and the postsynaptic neuron  $i$ , and  $s_j^{(t-1)}$  is a binary variable denoting the spikes of neuron  $j$  at time step  $t - 1$ .

To estimate the control error (difference between actual and desired value), we employed a pair of *PPC* neurons (*ePPC*) at each timestep. These two neurons receive the current-encoded values of  $\theta$  and  $\theta^d$  as input and encode the sign and magnitude of the error in their spiking activity. To encode the sign, we connected the four CCMs to the two *ePPC* in a way that enforces the mutually exclusive firing of the neurons. For example, when  $0 < \theta < \theta^d$ , only the two middle CCMs produced non-zero output, with the output of the bottom one being larger in magnitude. Connecting the two CCMs with both *ePPC* but with opposite signs ensures that *ePPC*<sup>-</sup> was excited, while the bottom one was shunted. In that way, *ePPC*<sup>-</sup> (*ePPC*<sup>+</sup>) was always active (inactive) when  $\theta < \theta^d$ . Following the same logic, we chose the rest of the connections between the CCM and the *ePPC*. The magnitude of the error was reflected by the

firing rate of the respective *ePPC*. The aggregate current from the CCM that stimulates the *ePPC* was proportional to the error, inducing a proportional firing rate in the neurons. In the above example, *ePPC*<sup>-</sup> was stimulated by a positive current proportional to  $\theta^d$  and a negative current proportional to  $\theta$ . Therefore, its firing rate was proportional to  $\theta^d - \theta$ .

To improve the control smoothness, we utilize another pair of *PPC* neurons (*dPPC*) that are sensitive to the rate of change of the control variable. These neurons introduce some push-pull dynamics: when  $\theta$  diverges considerably from  $\theta^d$ , the controller attempts to quickly decrease the error, giving rise to a sizeable derivative value. This value is input to the respective *dPPC* and activates it to counteract the error decrease and avoid overshooting. To incorporate the sensitivity of the *dPPC* to the rate of change of the control variable, we first estimated the derivative of  $\theta$  (measured its change over a time window and divided by the window length). Then, we encoded its value into a current, which was fed to the two *dPPC* with opposite signs. In that way, these neurons fire in a mutually exclusive manner to encode positive and negative rates of change, with their firing rate encoding the magnitude of the derivative.

3) *Actuation*: The actuation component of our network comprised of two antagonistic motor neurons, an extensor (E) and a flexor (F), that increased and decreased the control variable, respectively. The E integrated the spikes of the top *ePPC*, whose activity indicated a negative error ( $\theta < \theta^d$ ), and responded with spikes that increased  $\theta$  towards the target  $\theta^d$ . For this, we translated each E spike to an incremental increase of  $\theta$ . Concurrently, the E integrated the spikes of the left *dPPC*, whose activity indicated a decrease in  $\theta$  and responded with spikes to counteract that decrease. The connectivity and the function of the F neuron were analogous for the decrease of the control variable.

4) *Weight adaptation*: To improve the motion smoothness without sacrificing control accuracy, we introduced two time-dependent, multiplicative factors  $f^{(t)}$  and  $g^{(t)}$  that adapted the static synaptic weights  $W$  between the *ePPC* and the motor neurons, as shown below:

$$w^{(t)} = W \cdot f^{(t)} \cdot g^{(t)}, \quad (3)$$

To maximize the smoothness of the motion, we first introduced a biologically plausible, activity-dependent facilitation of the synaptic weights [32]. The efficacy  $f_{ij}^{(t)}$  of the synaptic connection between the  $j^{\text{th}}$  *ePPC* and the  $i^{\text{th}}$  motor neuron increased with each presynaptic spike until saturating at a maximum value and decayed otherwise with a factor  $d_{fac}$ , as shown in Eq. 4.

$$f_{ij}^{(t)} = f_{ij}^{(t-1)} \cdot d_{fac} + U_{fac} \cdot s_j^{(t-1)}, \quad (4)$$

Due to the low initial synaptic efficacies, abrupt increases in the activity of the *ePPC* do not directly propagate to the motor neurons. The gradual increase of the synaptic efficacies results in a graded activation of the motor neurons, resulting in a smooth modification of the controlled amount.

To maximize the control accuracy, we aimed to optimize the controller parameters according to the range of the desired movement. Specifically, while small errors require strong synaptic connections from the *ePPC* to activate the motor neurons and ensure accurate control, large errors require weaker connections to avoid overshoot. To address this requirement, we introduced the biologically plausible adaptation mechanism of presynaptic inhibition [22], and scaled the synaptic weights as a function of the error magnitude. Specifically, we utilized an additional neuron (PSI), whose activity reflected the activity of the *ePPC* and, therefore, the magnitude of the error. The PSI spikes modulated the connection weights as described below:

$$g^{(t)} = g_{max} - \left[ g^{(t-1)} \cdot d_{PSI} + U_{PSI} \cdot s_{PSI}^{(t-1)} \right], \quad (5)$$

where  $g$  was decreased by  $U_{PSI}$  with each PSI spike  $s_{PSI}^{(t-1)}$  and otherwise decayed to its maximum value  $g_{max}$  with a factor  $d_{PSI}$ . In that way, we emulated the divisive effect of presynaptic inhibition on the weights of biological synapses [22].

### B. Neuromorphic Realization

To demonstrate the applicability of our controller to neuromorphic hardware, we deployed our SNN architecture on Intel’s Loihi [11]. Due to its biologically plausible architecture, our SNN could be directly introduced to the hardware (Fig. 3, B). We implemented *PPC* and actuation neurons as single Loihi compartments governed by the Leaky Integrate and Fire (LIF) dynamics (Eq. 1-2) that Loihi inherently supports.

One limitation of the Loihi hardware is that it does not directly support facilitatory synapses. To overcome this limitation, we developed a facilitatory module. We designed this module as a two-compartment neuron that followed the imbalanced tree structure of multi-compartment neurons on Loihi. The leaf (small circle) is a non-spiking compartment that receives and integrates the module’s input. The root (large circle) is a spiking compartment that integrates the leaf compartment’s voltage. This cascaded integration of the input resulted in a gradual increase in the spiking activity of the root compartment, which induced gradual activation of the motor neurons, approximating the effects of the facilitatory synapses in our off-chip controller.

While this design introduced more Loihi compartments and connections than the number of neurons and synapses in the CPU-based implementation, our single-joint controller only required 10 compartments and 8 connections (60 compartments and 66 connections including the joint coordination for the control of the real-world Jaco arm). Therefore, the biological plausibility of the architecture minimized the resources requirements of our controller design.

### C. Multi-DOF Control

To scale up our single-DOF control approach and allow for the control of real-world robotic arms with multiple DOF, we used our SNN as a control block and independently applied it to each DOF of the arm’s joints. We drew inspiration from

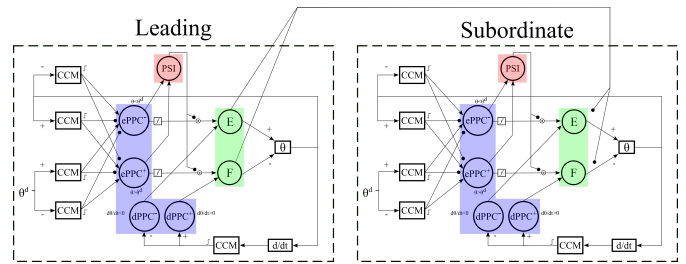


Fig. 3. Coordination of independent joint controllers.

the experimentally observed joint coordination in human arms and applied these principles in our arm controllers to improve the control behavior. Specifically, we incorporated the leading joint hypothesis [33], which postulates that in human arms, the joints that are closer to the body lead the movement, and the ones further down the limb (subordinate) follow. In that way, the subordinate joints exploit the leading joint’s inertia. To account for this, we stimulated the motor neurons of the subordinate joint with the spikes of the leading joint motor neurons. For the Reacher-v2, we defined the first joint (shoulder) as leading and the second (elbow) as subordinate. For the Jaco arm, we defined the first and second joints as leading and the remaining four as subordinate.

### D. Controller-Robot Interaction

To allow for our SNN to control the robot arms, we translated each spike of the motor neurons to an incremental change (positive for E and negative for F) in the angle of the respective joint. For the Reacher-v2, we first ran a calibration simulation to determine the nominal torques that are required to change each joint angle by the desired increment. Then, we translated each *E/F* spike during the arm control to a positive/negative torque increment of that magnitude. For the Jaco2 arm, we used our SNN to control the angle of each joint in the configuration space. Here, we predefined an angle increment and translated each spike of *E/F* to an increase/decrease of the respective angle by that increment. Then, we translated the instructed angles to torques using an analytic operational space controller [34].

The interaction between Loihi and the simulation environments was realized using the framework proposed in [35] to allow for real-time control of the robot arms (Fig. 4). For this, we used a Read channel controlled by the low-frequency x86 Loihi cores (SNIP) to read out the spiking activity of the motor neurons and translate it to joint movements. In Real-time estimates of  $\theta$  and  $d\theta/dt$  were fed as inputs to

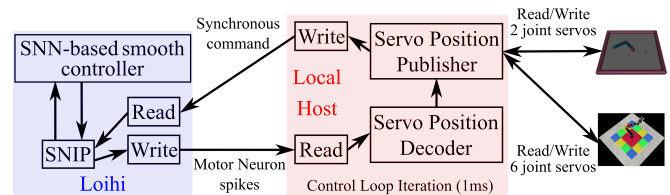


Fig. 4. Loihi-robot interaction control loop. Loihi communicates with the Local Host through a Read and a Write channel controlled by the on-chip x86 core (SNIP). The neuron spikes are decoded and used to update the simulated servos. The servo states are read out and fed back to Loihi.

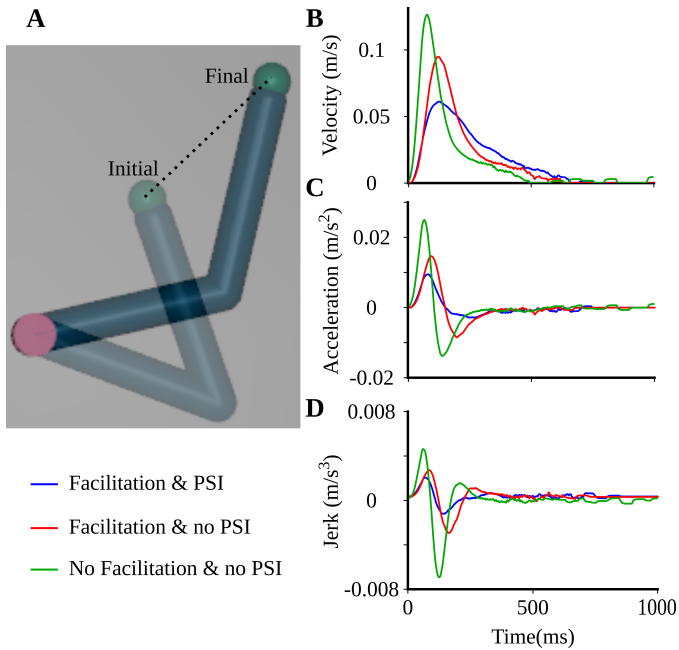


Fig. 5. Contribution of each network component to the improvement of the control smoothness. The SNN controller without facilitation and/or presynaptic inhibition (green and red) successfully drives the discrete movement, but gives rise to fast and abrupt end-effector movements (B, C). The complete SNN controller (blue) maximizes (minimizes) the control smoothness (jerk) (D).

the corresponding *PPC* neurons through a Write channel, which set the biases of these *PPC* neurons.

#### IV. RESULTS

##### A. Demonstrating smooth control and identifying its origins

Providing smooth control was one of the main goals of our design. As a proof of concept, we used our SNN controller to drive a discrete movement of the end effector of the Reacher-v2 arm (Fig. 5, A). To quantify the smoothness of our control approach, we computed a well-established smoothness metric [36] the motion jerk (the second derivative of the motion velocity Fig. 5), . We show the recorded trajectory and the evaluation metrics (joint velocity, acceleration, and jerk) after a single simulation because the absence of stochastic components in our method did not introduce any intra-session variability. Mimicking the behavior of its biological counterpart [22], our controller gave rise to bell-shaped velocity profiles (Fig. 5, B). The gradual acceleration and timely deceleration of the end-effector (Fig. 5, C) confined the magnitude of the motion jerk (Fig. 5, D), suggesting that our SNN indeed provided smooth control of the robotic arm.

To determine the contribution of each component of our SNN to the desired control behavior, we sequentially ablated the mechanisms and evaluated the control dynamics. First, we deactivated the adaptation mechanism of PSI and used the modified SNN controller to drive the exact same discrete movement. While the initial phase of the movement was unaffected in the absence of PSI, the peak end-effector velocity was not adequately confined (Fig. 5, B, red vs. blue curves). The deceleration from this higher peak velocity was

more abrupt (Fig. 5, C), leading to an increase in the motion jerk (both in terms of absolute magnitude and integral). Next, we deactivated both the PSI and the synaptic facilitation mechanisms, and the remaining SNN drove the same discrete movement. In the absence of the two mechanisms, both the increase and the decrease in the end-effector speed were abrupt, and the peak velocity was even higher (Fig. 5, B, green vs. blue curve). The consequent larger values of acceleration (Fig. 5, C) resulted in significantly increased motion jerk (Fig. 5, D).

##### B. Biological relevance of the motion trajectories

The biological inspiration of our SNN architecture made us wonder whether the resultant arm movements were similar to those observed in human arms. To examine this, we applied our controller to the Reacher-v2 arm to drive a sequence of discrete movements and recorded the trajectories of its end-effector (Fig. 6). At predefined intervals and regardless of the completion of the previous movements, a new, random goal position was defined for the end-effector. This workspace position was provided to an Inverse Kinematics (IK) solver that calculated the joint configuration that would drive the robot arm to the desired position. Then, the resulting angles were fed to the SNN controllers of the respective joints to drive their movements. As expected, our SNN controller provided smooth control with a gradual initial increase and timely decrease in the end-effector speed (as shown by the increased point density around the targets). Interestingly, the trajectories generated by our controller were not straight but had a sigmoid-shaped curvature that is characteristic of human arm movements [37]. Considering that our controller did not include motion planning beyond the calculation of the initial and final joint configurations, this natural emergence of slightly curved trajectories suggested that this human-like behavior resulted from our biologically plausible SNN architecture.

##### C. Application to multi-DOF robot arms

To demonstrate the applicability of our approach to real-world robotic arms, we scaled up our SNN to control a Jaco arm with 6 DOF. We used one controller block for

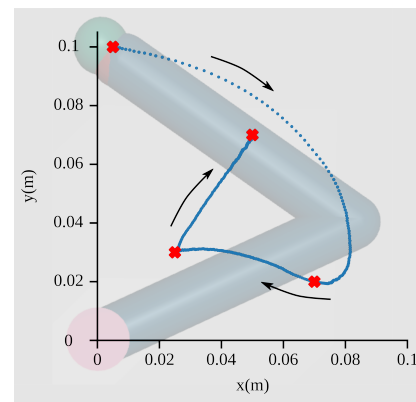


Fig. 6. End-effector trajectory for the 2-link arm when driven by the SNN controller to perform discrete movements. The curvature of the trajectories is in agreement with experimental evidence in human arms (see [37], Fig.2)

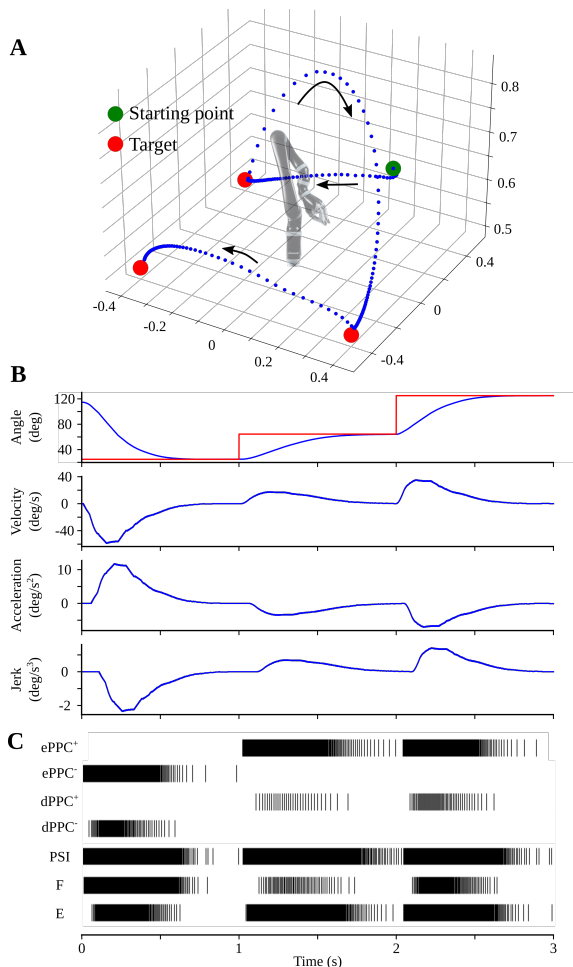


Fig. 7. SNN controller drives a Jaco arm. A. End-effector trajectory of the of the Jaco arm while performing discrete movements in the configuration space. The increased density of points around the targets shows the smooth acceleration and deceleration in the early and late stages of the movements. B. Control dynamics for an exemplary arm joint. C. Raster plot of the neuronal spiking activity that controls the joint in B.

each joint and introduced joint coordination as previously described. Here, the first joint of the arm acted as leading for the second, and both of them acted as leading for the other four. In that way, we exploited the inertia of the first joint in the x-y plane and the inertia of the second joint along the z-axis. We utilized our SNN controller to drive the discrete movement of the arm’s end-effector between three points in the workspace and recorded its trajectory (Fig. 7, A). As in the Reacher-v2 experiment, a new, random position for the end-effector was generated at predefined time instances and regardless of the completion of previous movements. Then, the IK solver for the Jaco arm transformed the workspace positions to joint configurations, and the target joints were fed to the respective controllers to drive the arm to the desired position. As discussed above, we only show the results of a single simulation since there was no variability across simulations. As in the case of the Reacher-v2 arm, the end-effector trajectory was smooth, with gradual deceleration when approaching the targets. This behavior of the end-effector was a result of the smooth control of each

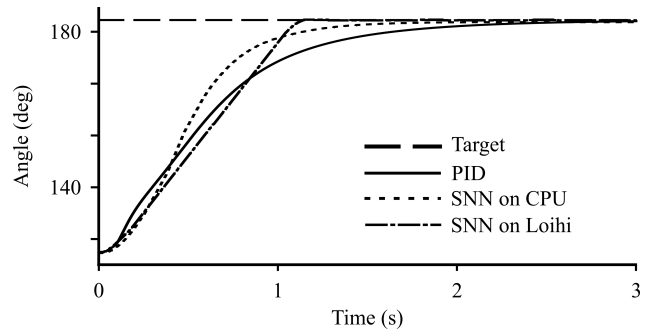


Fig. 8. Performance comparison between the SNN and a PID controller. Both controllers give rise to similar step responses when controlling a single joint of the Jaco arm. Quantitative comparison of the different controller metrics are shown in Table I.

joint separately. As an example, we show the dynamics of one arm joint controlled by our SNN (Fig. 7, B). The joint moved accurately and smoothly to the desired angles without overshoot (Fig. 7, B, top panel) while preserving the bell-shaped angular speed profiles (Fig. 7, B, middle panel) that kept the motion jerk to minimal levels (Fig. 7, B, bottom panel). The spiking activity of the neurons in the respective SNN controller block explains the control dynamics of the single joint (Fig. 7, C). Specifically, for each step movement, one of the *ePPCs* was activated by the position error and drove its respective motor neuron (*E/F*) to decrease it. As the joint started moving towards the target, the respective *dPPC* was activated due to the change in the angular speed and, in turn, stimulated the antagonist motor neuron (*F/E*). This counteraction resulted in a timely joint deceleration when approaching the target, contributing to the smoothness of the control. Lastly, the *PSI* neuron contributed to the fine-tuning of the movement: This neuron was highly active in the early stages of the movement when the positional error was high. In that way, it downscaled the synaptic weight between the *ePPCs* and the motor neurons to avoid the overshoot induced by strong *E/F* activation. As the error decreased towards the end of the movement, the activity of *PSI* faded, allowing for the gradual increase of the synaptic weight to its maximal value. The larger weight was then sufficient to accurately correct the small positional errors without inducing overshoots.

#### D. Comparison with conventional PID control

After demonstrating that our SNN controller is indeed applicable to real-world robotic arms with multiple DOF, we evaluated our approach by comparing it with a state-of-the-art PID controller that is widely used in similar applications. We compared the step response of the two

TABLE I  
CONTROLLER METRICS COMPARISON

	Overshoot ( $\theta_{max} - \theta_{des}$ %)	Rise time (10% - 90% $\theta_{des}$ )	Settling Time ( $<20\%\theta_{des}$ )
PID	0	1136.9 ms	945.5 ms
SNN (CPU)	0	724.3 ms	723.8 ms
SNN (Loihi)	1.7	804 ms	881 ms

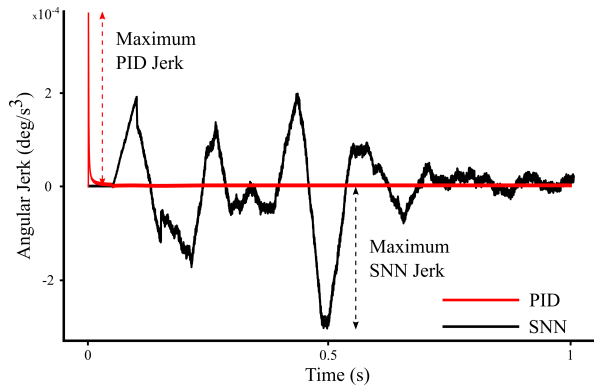


Fig. 9. Comparison of the end-effector’s jerk when driven by the SNN (black) and a PID (red) controller. The maximal jerk was lower for the SNN controller resulting in more smooth motion.

controllers when required to drive a single robot joint from an initial to a desired configuration (Fig. 8). Our SNN controller implemented on either a CPU or Loihi achieved comparable performance to the PID. We quantified this comparison by measuring the overshoot, the rise time, and the settling time of the controllers (Table I). Our SNN controllers exhibited a similar rise and settling time with the PID. While the SNN controllers were slightly faster than the PID, we clarify that our goal was not to outperform the conventional control method but to achieve comparable results with a biologically plausible and, therefore, neuromorphic-compatible approach. When implemented on Loihi, the SNN controller exhibited a small (1.7%) overshoot which was absent in the CPU implementation. This was expected due to the absence of presynaptic inhibition in our Loihi deployment, which further highlights the contribution of this adaptation mechanism to the control.

With motion smoothness being the main goal for our controller design, we further examined this aspect of its performance and compared it with the state-of-the-art PID controller. Both controllers drove the same discrete movement of the Jaco arm (Section IV.D) and we evaluated the motion smoothness (Fig. 9). To do so, we used the well-established jerk metric (derivative of the acceleration) [38], which is minimal in smooth human arm movements [18]. When using the PID controller, an initial spike dominated the motion jerk, which quickly decayed to zero subsequently. On the other hand, our SNN controller gave rise to a gradual increase in the motion jerk that persisted longer, decreasing the maximum jerk by 19%. With jerk quantifying how abrupt the movement is, high instantaneous values deteriorate the movement smoothness more than smaller and persistent ones. Therefore, our method indeed improved motion smoothness, approximating the minimum jerk profiles in human arms.

## V. DISCUSSION

In this paper, we presented an SNN controller which draws inspiration from biological findings on how primates perform smooth reaching movements [22]. We evaluated our controller on two robotic arms: i) the simple but human-like two-link arm Reacher-v2, and ii) the real-world 6-DOF

Jaco arm. Our results show that the controller not only drove the arm to the target accurately but also provided smooth control, thus making it applicable for a wide variety of robotic applications, such as prosthetics [5], assistive arms [2], or industrial arms [3], that may require such control.

Adding to the mounting evidence that demonstrates the role of neuroscience in advancing robotics [23], [39]–[42], we show here how an understanding of how the brain achieves the desired behavior can be translated into neuromorphic solutions. Several recent studies have attempted to harness the advantages of neuromorphic platforms for low-level control [15]–[17]. Their performance approximates that of the conventional microcontrollers, showing that the non-Von Neumann architecture of the hardware is not a compounding factor. However, the deployment of conventional control methods on neuromorphic hardware disregards the underlying neuroscience principles. As a result, such methods only partially exploit the low complexity of the minimal brain networks. Here, we propose an SNN controller whose architecture faithfully follows the connectivity of the brain circuits that provide smooth reaching movements in primates [21] and rodents [22]. This biological plausibility not only resulted in a minimal network in terms of size and complexity but also made it a perfect fit for deployment on neuromorphic hardware. Functionally, the controller inherited the behavior of its biological counterpart, as control smoothness emerged naturally through the gradual increase and timely and steady decline of the controlled variable.

While the biologically inspired design of our SNN controller resulted in the above mentioned architectural and functional advantages, it also gave rise to some limitations. First, our controller, similarly to other SNN solutions, lacks the concrete mathematical description of a PID controller. Drawing inspiration from biological networks controlling reaching movements, our SNN design is interpretable at the behavioral level. However, a thorough analysis of the control behavior is less straightforward when compared to conventional control methods. Second, our SNN controller introduced more tunable parameters than the three PID coefficients. Although the behaviorally interpretable nature of our design simplifies the tuning of the network hyperparameters, their increased number introduces additional complexity. Lastly, the binary nature of our spiking controller might introduce limited flexibility when compared with a continuous conventional controller. However, our method could be expanded with and benefit from previously proposed SNN controllers [28] that attempt to overcome this limitation.

Overall, this work supports ongoing efforts to develop real-time and robust control solutions that can exhibit desired behaviors. The work aims to derive computational principles from the knowledge of how the brain exhibits optimal motor behavior and introduce them to the design of neuromorphic controllers for robots. In the light of our results, which combine performance comparable with the state-of-the-art with low computational complexity and interpretability, the direction of developing brain-inspired neuromorphic solutions to robotic problems is worth exploring further.

## REFERENCES

- [1] D. Erol and N. Sarkar, "Smooth human-robot interaction in robot-assisted rehabilitation," in *2007 IEEE 10th International Conference on Rehabilitation Robotics*. IEEE, 2007, pp. 5–15.
- [2] I. Naotunna, C. J. Perera, C. Sandaruwan, R. Gopura, and T. D. Lalitharatne, "Meal assistance robots: A review on current status, challenges and future directions," in *2015 IEEE/SICE International Symposium on System Integration (SII)*. IEEE, 2015, pp. 211–216.
- [3] Y. Xiao, Z. Du, and W. Dong, "Smooth and near time-optimal trajectory planning of industrial robots for online applications," *Industrial Robot: An International Journal*, 2012.
- [4] J. Rivera-Guillen, R. Romero-Troncoso, A. Osornio-Rios, A. Garcia-Perez, and I. Torres-Pacheco, "Extending tool-life through jerk-limited motion dynamics in machining processes: An experimental study," 2010.
- [5] L. R. Hochberg, M. D. Serruya, G. M. Friehe, J. A. Mukand, M. Saleh, A. H. Caplan, A. Branner, D. Chen, R. D. Penn, and J. P. Donoghue, "Neuronal ensemble control of prosthetic devices by a human with tetraplegia," *Nature*, vol. 442, no. 7099, pp. 164–171, 2006.
- [6] H. I. Krebs, N. Hogan, M. L. Aisen, and B. T. Volpe, "Robot-aided neurorehabilitation," *IEEE transactions on rehabilitation engineering*, vol. 6, no. 1, pp. 75–87, 1998.
- [7] I. Maurtua, A. Ibaruren, J. Kildal, L. Susperregi, and B. Sierra, "Human-robot collaboration in industrial applications: Safety, interaction and trust," *International Journal of Advanced Robotic Systems*, vol. 14, no. 4, p. 1729881417716010, 2017.
- [8] F. Rubio, F. Valero, and C. Llopis-Albert, "A review of mobile robots: Concepts, methods, theoretical framework, and applications," *International Journal of Advanced Robotic Systems*, vol. 16, no. 2, p. 1729881419839596, 2019.
- [9] T. Taunyazov, W. Sng, H. H. See, B. Lim, J. Kuan, A. F. Ansari, B. Tee, and H. Soh, "Event-driven visual-tactile sensing and learning for robots," in *Proceedings of Robotics: Science and Systems*, July 2020.
- [10] N. Imam and T. A. Cleland, "Rapid online learning and robust recall in a neuromorphic olfactory circuit," *Nature Machine Intelligence*, vol. 2, no. 3, pp. 181–191, 2020.
- [11] M. Davies, N. Srinivasa, T.-H. Lin, G. Chinya, Y. Cao, S. H. Choday, G. Dimou, P. Joshi, N. Imam, S. Jain *et al.*, "Loihi: A neuromorphic manycore processor with on-chip learning," *IEEE Micro*, vol. 38, no. 1, pp. 82–99, 2018.
- [12] P. A. Merolla, J. V. Arthur, R. Alvarez-Icaza, A. S. Cassidy, J. Sawada, F. Akopyan, B. L. Jackson, N. Imam, C. Guo, Y. Nakamura *et al.*, "A million spiking-neuron integrated circuit with a scalable communication network and interface," *Science*, vol. 345, no. 6197, pp. 668–673, 2014.
- [13] C. Mayr, S. Hoepfner, and S. Furber, "Spinnaker 2: A 10 million core processor system for brain simulation and machine learning," *arXiv preprint arXiv:1911.02385*, 2019.
- [14] M. Davies, A. Wild, G. Orchard, Y. Sandamirskaya, G. A. F. Guerra, P. Joshi, P. Plank, and S. R. Risbud, "Advancing neuromorphic computing with loihi: A survey of results and outlook," *Proceedings of the IEEE*, vol. 109, no. 5, pp. 911–934, 2021.
- [15] A. L. Christensen and Y. Sandamirskaya, "Event-based pid controller fully realized in neuromorphic hardware: a one dof study."
- [16] J. Zhao, N. Risi, M. Monforte, C. Bartolozzi, G. Indiveri, and E. Donati, "Closed-loop spiking control on a neuromorphic processor implemented on the icub," *IEEE Journal on Emerging and Selected Topics in Circuits and Systems*, vol. 10, no. 4, pp. 546–556, 2020.
- [17] Y. Zaidel, A. Shalunov, A. Volinski, L. Supic, and E. E. Tsur, "Neuromorphic nef-based inverse kinematics and pid control," *Frontiers in Neurobotics*, vol. 15, 2021.
- [18] T. Flash and N. Hogan, "The coordination of arm movements: an experimentally confirmed mathematical model," *Journal of neuroscience*, vol. 5, no. 7, pp. 1688–1703, 1985.
- [19] I. Q. Whishaw, "An endpoint, descriptive, and kinematic comparison of skilled reaching in mice (*mus musculus*) with rats (*rattus norvegicus*)," *Behavioural Brain Research*, vol. 78, no. 2, pp. 101–111, 1996.
- [20] E. Todorov, "Optimality principles in sensorimotor control," *Nature neuroscience*, vol. 7, no. 9, pp. 907–915, 2004.
- [21] K. Seki, S. I. Perlmutter, and E. E. Fetz, "Sensory input to primate spinal cord is presynaptically inhibited during voluntary movement," *Nature neuroscience*, vol. 6, no. 12, pp. 1309–1316, 2003.
- [22] A. J. Fink, K. R. Croce, Z. J. Huang, L. Abbott, T. M. Jessell, and E. Azim, "Presynaptic inhibition of spinal sensory feedback ensures smooth movement," *Nature*, vol. 509, no. 7498, pp. 43–48, 2014.
- [23] I. Polykretis, G. Tang, and K. P. Michmizos, "An astrocyte-modulated neuromorphic central pattern generator for hexapod robot locomotion on intel's loihi," in *International Conference on Neuromorphic Systems 2020*, 2020, pp. 1–9.
- [24] I. Polykretis, G. Tang, P. Balachandar, and K. P. Michmizos, "A spiking neural network mimics the oculomotor system to control a biomimetic robotic head without learning on a neuromorphic hardware," *IEEE Transactions on Medical Robotics and Bionics*, pp. 1–10, 2022.
- [25] R. Kreiser, A. Renner, V. R. Leite, B. Serhan, C. Bartolozzi, A. Glover, and Y. Sandamirskaya, "An on-chip spiking neural network for estimation of the head pose of the icub robot," *Frontiers in Neuroscience*, vol. 14, 2020.
- [26] G. Luo and G. Saridis, "Lq design of pid controllers for robot arms," *IEEE Journal on Robotics and Automation*, vol. 1, no. 3, pp. 152–159, 1985.
- [27] H. A. Malki, D. Misir, D. Feigenspan, and G. Chen, "Fuzzy pid control of a flexible-joint robot arm with uncertainties from time-varying loads," *IEEE Transactions on Control Systems Technology*, vol. 5, no. 3, pp. 371–378, 1997.
- [28] A. Jimenez-Fernandez, G. Jimenez-Moreno, A. Linares-Barranco, M. J. Dominguez-Morales, R. Paz-Vicente, and A. Civit-Balcells, "A neuro-inspired spike-based pid motor controller for multi-motor robots with low cost fpgas," *Sensors*, vol. 12, no. 4, pp. 3831–3856, 2012.
- [29] R. K. Stagsted, A. Vitale, A. Renner, L. B. Larsen, A. L. Christensen, and Y. Sandamirskaya, "Event-based pid controller fully realized in neuromorphic hardware: a one dof study," in *2020 IEEE/RSJ International Conference on Intelligent Robots and Systems (IROS)*. IEEE, 2020, pp. 10939–10944.
- [30] R. Stagsted, A. Vitale, J. Binz, L. Bonde Larsen, Y. Sandamirskaya *et al.*, "Towards neuromorphic control: A spiking neural network based pid controller for uav." RSS, 2020.
- [31] S. Glatz, J. Martel, R. Kreiser, N. Qiao, and Y. Sandamirskaya, "Adaptive motor control and learning in a spiking neural network realised on a mixed-signal neuromorphic processor," in *2019 International Conference on Robotics and Automation (ICRA)*. IEEE, 2019, pp. 9631–9637.
- [32] M. Tsodyks, K. Pawelzik, and H. Markram, "Neural networks with dynamic synapses," *Neural computation*, vol. 10, no. 4, pp. 821–835, 1998.
- [33] N. Dounskaia, "The internal model and the leading joint hypothesis: implications for control of multi-joint movements," *Experimental Brain Research*, vol. 166, no. 1, pp. 1–16, 2005.
- [34] O. Khatib, "A unified approach for motion and force control of robot manipulators: The operational space formulation," *IEEE Journal on Robotics and Automation*, vol. 3, no. 1, pp. 43–53, 1987.
- [35] G. Tang, N. Kumar, and K. P. Michmizos, "Reinforcement co-learning of deep and spiking neural networks for energy-efficient mapless navigation with neuromorphic hardware," *arXiv preprint arXiv:2003.01157*, 2020.
- [36] N. Hogan, "An organizing principle for a class of voluntary movements," *Journal of neuroscience*, vol. 4, no. 11, pp. 2745–2754, 1984.
- [37] J. Konczak and J. Dichgans, "The development toward stereotypic arm kinematics during reaching in the first 3 years of life," *Experimental brain research*, vol. 117, no. 2, pp. 346–354, 1997.
- [38] K. J. Kyriakopoulos and G. N. Saridis, "Minimum jerk path generation," in *Proceedings. 1988 IEEE international conference on robotics and automation*. IEEE, 1988, pp. 364–369.
- [39] Y. Sandamirskaya, M. Kaboli, J. Conrad, and T. Celikel, "Neuromorphic computing hardware and neural architectures for robotics," *Science Robotics*, vol. 7, no. 67, p. eabl8419, 2022.
- [40] J. Dupeyroux, S. Stroobants, and G. de Croon, "A toolbox for neuromorphic sensing in robotics," *arXiv preprint arXiv:2103.02751*, 2021.
- [41] P. Manoonpong, U. Parlitz, and F. Wörgötter, "Neural control and adaptive neural forward models for insect-like, energy-efficient, and adaptable locomotion of walking machines," *Frontiers in neural circuits*, vol. 7, p. 12, 2013.
- [42] A. J. Ijspeert, "Central pattern generators for locomotion control in animals and robots: a review," *Neural networks*, vol. 21, no. 4, pp. 642–653, 2008.